Silicon (2019) 11:1295–1311
https://doi.org/10.1007/s12633-018-9920-2

ORIGINAL PAPER

Tribology Analysis of Cobalt Particulate Filled Al 7075 Alloy for Gear Materials: a Comparative Study

Ashiwani Kumar[1] · Amar Patnaik[1] · I. K. Bhat[2]

Received: 4 March 2017 / Accepted: 25 May 2018 / Published online: 21 June 2018

Abstract

The present study aims at developing a theoretical model for sliding wear analysis of the cobalt metal powder reinforced Aluminum (Al7075) alloy composites and perform an experimental run for validation of the theoretical model. The alloy composites are fabricated in high temperature vacuum centrifugal casting set-up by varying the cobalt metal powder to analyze the effect of different weight fraction (0, 0.5, 1.5, and 2.0 wt.-% cobalt metal powder) of cobalt metal powder on wear and coefficient of friction analysis under different operating conditions(such as Normal load (20N-80N), Sliding speed (0.25m/s-1.25m/s) and Sliding distance (250 m-1250 m).Finally, the specificwear rate of the alloy composites is studied experimentally to get the wear rate and coefficient of friction of the alloy composites. At the end, the worn surface morphology of the alloy composites is studied by using scanning electron microscopic to understand the type of wear failure in different operating medium.

Keywords Aluminum alloys · Friction and wear · Surface modification · Cobalt particulate · Theoretical model

Nomenclature

HV Vickers hardness
NIMP Nickel metal powder
TIMP Titanium metal powder
COMP Cobalt metal powder
CRMP Chromium metal powder
AACO-0 Unfilled Aluminum alloy composite
AACO-0.5 Aluminum alloy composite reinforced with 0.5% Cobalt metal powder
AACO- 1 Aluminum alloy composite reinforced with 1 % Cobalt metal powder
AACO-1.5 Aluminum alloy composite reinforced with 1.5% Cobalt metal powder
AACO-2.0 Aluminum alloy composite reinforced with 2 % Cobalt metal powder

✉ Amar Patnaik
patnaik.amar@gmail.com

[1] Mechanical Engineering Department, M.N.I.T., Jaipur, 302017, India

[2] Applied Mechanics Department, M.N.N.I.T, Allahabad, U.P. 211004, India

1 Introduction

Aluminum matrix composites (AMCs) are considered to be superior alternative over conventional materials for structural applications in aeronautical, aerospace, automobile, defense etc. owing to their superior properties such as strength, toughness, hardness, impact energy, flexural strength and higher wear resistance etc. respectively [1]. Such significant research are advocated by various research scientist worldwide, like Ralph et al. [2] reported that with increase in volume fraction of particulate reinforcement the elastic modules observed to shown increasing trend as compare to neat alloy. Similarly, Kumar et al. [3] observed that the behavior of composite material under various environmental conditions could be predicted based upon constituents intrinsic properties; structural arrangement and interaction among constituents. The Gangwar et al. [4] observed an increase in hardness, density and void content while decrease in impact strength when A384 alloy composite is reinforced with micro TiO_2, however the same alloy shows reduction in void contents / density while impact energy / hardness increases when reinforced with nanoTiO_2. The alumina (Al_2O_3) reinforcement is reported to boost the physical and mechanical behavior (such as tensile strength, flexural strength, impact strength and hardness) of aluminum alloy composites by Kukshal et al. [5].

Similar observations is made by Baradeswaran and Perumal [6] with B_4Ccontent and Kumar et al. [7] with SiC/Al_2O_3. Komai et al. [8] reported superior mechanical characteristics Al7075–SiCcomposites.Savaskan and Alemdag [9] investigated the effects of nickel particulates additions on Al–40Zn–3Cu alloy and reported better wear resistance of the alloy composite Rajeev et al. [10] investigated reinforcement of 15 wt.% silicon carbide contents on Al–Si–SiC_p alloy composites under dry sliding condition and observed that the specific wear rate increases with increase in the normal load from 60-120 N respectively whereas, the coefficient of friction shows reverse trend. The specific wear rate of the Al7075/Al_2O_3 metal composites will increases in load range 10-40 N as reported by Baradeswaran et al. [11]. Ravindran et al. [12] found increase in wear loss of Al-2024/ 5wt% SiC/x wt% Gr (x = 0, 5, and 10) hybrid composite with load (up to 40 N). Kumar and Dhiman [13] found that the hybrid composites show higher wear resistance with filler content than the alloy matrix over the complete range of applied load (20-60 N).Similar, observations are reported by Kiran et al. [14] and Li et al. [15] found wear behavior of Al6061/SiC/ Al_2O_3 of hybrid metal matrix composite. It noticed that high wear resistance of alloy composites and low coefficient friction of alloy composite. Nwambu et al. [16] and Sani et al. [17] investigated that effect of Mo Cr and Co addition on structure and mechanical properties of Al 12.5% Si alloy. It is observed that the hardness, impact strength and corrosion wear resistance improve with addition Cobalt filler content and microstructure result shows the fine distribution of Cobalt particles. Similar observation is made by Haq et al. [18] with Si3N4 content and Kumar et al. [19, 20] with Ni and Ti content. It is noticed that hardness and wear resistance improves with increase in filler content.

In light of above research reports, in this research work, study of physical and tribological behavior of Al7075 alloy composite reinforced with cobalt powder is reported and subsequently wear mechanisms are studies using SEM micrographs.

2 Proposed Theoretical Wear Model for Gear

During gear meshing, gear surfaces undergo sliding wear process from engagement to disengagement of teethes. Consequently, instant flash temperature will be generated due to contact and frictional heat that causes material loss or wear loss (termed as gear tribology). Experimentally, we can simulate this two-body wear mechanism on pin-on-disk tribo-tester (pin made of composite alloy material). The complete gear tribology is function of many variables like tangential tooth load, normal load, rotational speed, material etc. The available mathematical model to predict wear loss during gear meshing seldom considered tangential tooth load and coefficient of friction. The proposed model will consider all such factors into consideration. The wear rates are computed using Archard's [21–24] Eq. 1, which states that wear rate (i.e. volumetric wear per unit sliding distance) is directly proportional to the applied normal load (W) and inversely proportional to hardness (H) of the material.

$$Q = \frac{KW}{H} \tag{1}$$

where, 'Q' is the volumetric wear per unit sliding distance, 'W' is the applied load, 'H' is the material hardness and 'K' is the wear coefficient. Also, wear rate is independent of apparent contact area.

At macroscopic level, the complex wear phenomenon occurs at interacting asperities, elastic and plastic deformation of asperities etc [25–27]. During contact condition of asperities there is temporary metal-to-metal joining due to atomic diffusion across metal boundaries. There are several such contact points that exists, with each contact point having a small specific surface area denoted by Ap and expressed in Equation.

$$A_P = \frac{P_P \cdot A_C}{K_r} \tag{2}$$

where, 'P_P' is the mean effective pressure at that point, and 'K_r' is constant that relates the real contact area to the load applied which is equivalent to hardness of the material. The whole contact area may or may not yield depending upon load and contact. Let A_{ci} and A_p be the two asperity areas such that number of asperities (N_n) in contact will be given by Equation.

$$N_n = \frac{P_P \cdot A_p}{K_r \cdot A_{Ci}} \tag{3}$$

Further, worn-off volume (V_i) of asperities is proportional to contact area and sliding distance (s). It is computed by Equation and the sliding distance is the function of time period of contact, probability of contact with another asperity and velocity.

$$V_i = C_{wm} \cdot A_{Ci} \cdot C_{top} \cdot S \tag{4}$$

where, C_{wm} denotes the wear mechanism, C_{top} denotes the probability of contact, sis the sliding distances between the two adjacent point of the interacting surface and A_{ci} is the real contact area of asperity i. The total wear volume in A_P will then be the sum of all V_i in A_P according to Equation

$$V_{AP} = V_i \cdot N_n = \frac{P_P \cdot A_p}{K_r \cdot A_{Ci}}.\ C_{wm} \cdot A_{Ci} \cdot C_{top} \cdot S \tag{5}$$

Differentiating Eq. 5 with respect to $s$then it becomes Equation.

$$\frac{dV_{AP}}{ds} = \frac{P_P \cdot A_p}{K_r}.\ C_{wm} \cdot C_{top} \tag{6}$$

If 'C_{top}' is equal to 1, 'K_r' is the constant, the hardness (H) of the softer surface and C_{wm} constant, then Eq. 6 can be formulated, if summed over every 'Ap', as Archard's wear Equation.

$$\frac{V}{s} = K\frac{W}{H} \tag{7}$$

where, 'V' is the wear volume of material, 'W' is the normal load applied, 'H' is the hardness of the surface under observation and 'K' is the wear coefficient [28].

To estimate the tangential tooth load [W_T]

According to Lewis theory, the applied normal load keeps on shifting from one gear profile to another gear profile in mesh. This normal load is uniformly distributed over the entire teeth profile. Consider cantilever beam of triangular cross-section fixed at B-t-C and loaded at point A as shown in Fig. 1. Considering free-body-diagram of forces, there are tangential components (W_T) acting perpendicular and radial component (W_R) acting parallel at the point-of-contact of pitch circles of the mating gears. The tangential force component may generate bending stresses leading to facture while, radial force component generates compressive stress of insignificant magnitude hence may be neglected. The part of highest bending stress may be computed by drawing a parabola through A and tooth graph at B and C as indicated in (Fig. 1).

The beam strength of the teeth geometry such as parabola, it will experience uniform stress. But the profile of tooth is bigger than the parabola at every point except *BC* hence experience highest stress. The highest bending stress at BC is computed by Equation

$$\sigma_w = \frac{M.y}{I} \tag{8}$$

Whereas

M = Highest bending moment at the section (BC) = $W_T \times$ h,
W_T = Tooth load (Tangential load)
h = Length (Tooth profile)

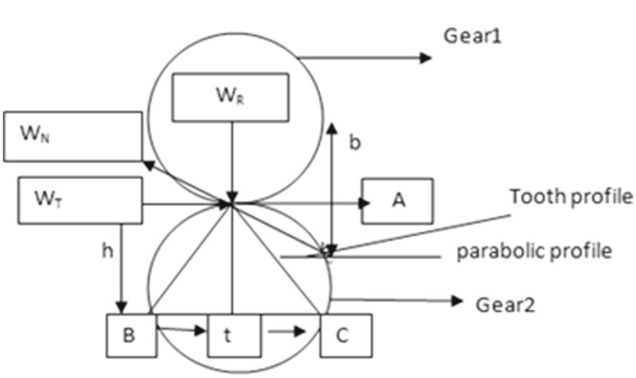

Fig. 1 Tooth geometry of gear

y = Half the thickness of the profile tooth (t) at section (BC) = t/2,
I = Moment of inertia (tooth) = $b.t^3/12$,
b = Width (gear face)

Substituting the values for M, y and I in Eq. 8 and simplifying, we get (9) and (10)

$$\sigma_w = (W_T.h)\frac{t.\ 12}{2bt^3} = (W_T.h)\frac{t.\ 6}{bt^3} \tag{9}$$

$$W_T = \sigma_w \cdot b \cdot \frac{t^2}{6h} \tag{10}$$

In this expression, tan dh is factors based upon the tooth profile size.

Let t = x.Pc and h = k. p_c, where x and k are constants and Substituting the values for t, hin (10), we get Equation

$$W_T = \sigma_w \cdot b \cdot p_c \cdot \frac{x^2}{6h} \tag{11}$$

Substituting x2 / 6h = y, and $p_c = \pi$m we have Equation

$$\begin{aligned} W_T &= \sigma_w \cdot b \cdot p_c \cdot \tfrac{x^2}{6h} = \sigma_w \cdot b \cdot p_c \cdot y \\ W_T &= \sigma_w \cdot b \cdot y \cdot \pi \cdot m \end{aligned} \tag{12}$$

The above equation modified as Equation given below.

$$W_T = \sigma_w \cdot C_V \cdot b \cdot p_c \cdot \pi \cdot m \cdot Y \cdot \frac{L-b}{L} \tag{13}$$

Whereas y is Lewis form factor and W_T (which is the Load of tangential acting at the profile of tooth).and putting the value of $W_n = W_{T/COS\varphi}$ in Eq. 7 we get Equation

$$\frac{V}{s} = K\frac{W_T}{H.COS\varphi} \tag{14}$$

Substituting the values for W_T in Eq. 14, we get Equation

$$\frac{V}{s} = K\frac{\sigma_w \cdot C_V \cdot b \cdot p_c \cdot \pi \cdot m \cdot Y \cdot (L-b)/L}{H.COS\varphi} \tag{15}$$

Where σ_w = Allowable static stress

C_Ve = Velocity factor
V = Peripheral speed in m / s,
B = Face width,
m = Module,
Y = Lewis factor
L = Distance of Cone

Simplify the Eq. 15, we get Equation

$$\frac{V}{s} = K\frac{\sigma_w \cdot C_V \cdot b \cdot \pi \cdot m \cdot Y \cdot S(L-b)/L}{H.COS\varphi} \tag{16}$$

Differentiate with respected to s, Eq. 16 becomes as Equation

$$\frac{dV}{ds} = K\frac{\sigma_w \cdot C_V \cdot b \cdot \pi \cdot m \cdot Y \cdot (L-b)/L}{H.COS\varphi} \tag{17}$$

Table 1 Chemical composition of Al7075 alloy (In weight percent)

Chemical Composition	Si	Fe	Cu	Mn	Mg	Cr	Zn	Ti	Al
Al7075	0.4	0.5	1.6	0.3	2.5	0.15	5.5	0.2	Bal

Substituting the values for ds = v.dt and σ_W = p/A in Eq. 17, we get

$$\frac{dV}{dt} = K\frac{P\cdot C_V\cdot b\cdot v\cdot\pi\cdot m\cdot Y\cdot t\cdot\frac{L-b}{L}}{t\cdot A\cdot H\cdot COS\varphi}$$

Therefore, the optimal theoretical volumetric wear rate of gear composite is shown in Equation

$$\frac{dV}{dt} = K\frac{P\cdot C_V\cdot b\cdot v\cdot\pi\cdot m\cdot Y\cdot t\cdot\frac{L-b}{L}}{H.COS\varphi} \quad (18)$$

Where $\frac{dV}{dt}$ = wear rate (mm^3/second)

P = Load for gear tooth (Newton)
V = sliding velocity of gear tooth (mm/second)
K= k/At = wear coefficient of bevel gear
t = sliding Contact time for bevel gear (seconds)

The mathematical expression in Eq. 18 may be utilized for predicting the volumetric wear loss of gear material in-conjunction with experimental wear loss.

3 Experimental Methods and Materials

3.1 Ingredients of the Investigated Composite Materials

The composite material developed for this research work (i.e. for pin samples) consists of (i) cobalt metal powder (0-2 wt.-% at steps of 0.5) as reinforcing element, (ii) Al-7075 alloy as matrix and cobalt particles size (325 mesh) was used. (Table 1 lists the chemical composition of alloy).

3.2 Fabrication of Composites

The composites specimens are fabricated on high temperature vertical vacuum furnace (Fig. 2). This equipment consists of heating chamber having (i) graphite crucible to have alloy metal pieces for melting (ii) a plunger (8mm diameter tip) for pushing molten metal into dies through pouring tubes in vacuum chamber (iii) temperature sensor to monitor temperature / heat inside the heating chamber (iv) magnifying glass eye-piece to check the activities inside the heating chamber.

The steps follows for fabrication are (i) pre-heating filler material (i.e. cobalt metal powder), base material (Al-7075

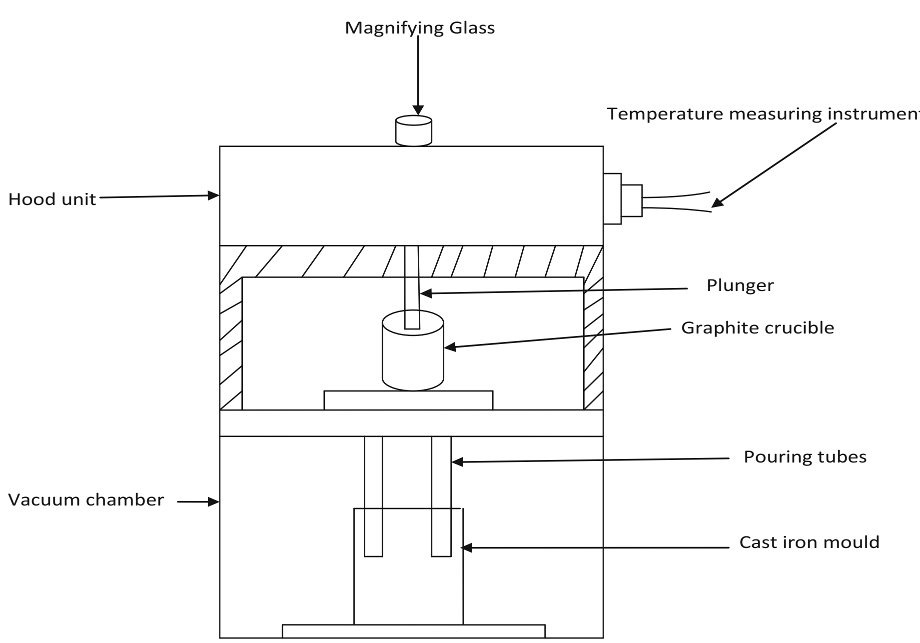

Fig. 2 Schematic diagram of high temperature vacuum casting machine

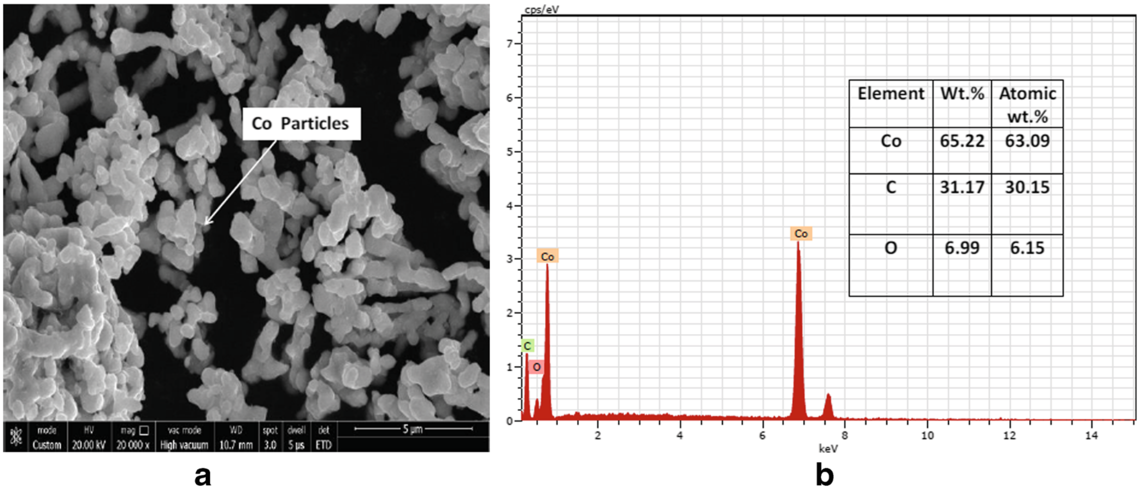

Fig. 3 Details of Co particles **a** SEM micrograph of Cobalt particles **b** EDX image of cobalt particles

alloy) and graphite crucible in heating chamber up to 160 °C. As and when the temperature of the base alloy material reaches above its liquids temperature i.e. 800 °C, about 2 wt.-% of magnesium is uniformly mixed in the molten alloy metal to improve wetablility (Fig. 3). Thereafter, pre-heated cobalt metal powder is added in the melt as per proportion and stirred homogeneous for at least 15 minutes. Once things are completed the plunger opened and the mixture drops vertically down into cast-iron mold (size: 140 × 90× 10 mm^3). The solidified specimens plates are taken out of mold and air quenched for several hours till temperature of the sample reaches to room temperature (Fig. 4). Thereafter, the Pin specimen size (13 mm× 9 mm× 10 mm) are polished and cut into various sample sizes for various characterizations like physical, mechanical and wear analysis.

3.3 Physical and Mechanical Characterization

The theoretical density of the specimens is computed as per Agarwal and Broutman rule of mixture [29] as per Eq. 19.For measuring actual density Archimedes principle is applied, first by weighing the specimen sample in air divided by rise of water level in the tube partially filled with water. Finally, void content is calculated using Eq. 20.

$$\rho t = \frac{1}{\frac{wr}{\rho\, r} + \frac{wm}{\rho m}} \tag{19}$$

$$\text{void fraction} = \frac{\text{theoretical}(\rho t) - \text{experimental}(\rho e)}{\text{theoretical}(\rho\ t)} \tag{20}$$

where, 'ρ_t', 'ρ_r', 'ρ_m' and 'ρ_e' represent the theoretical density, particulate density and matrix material density

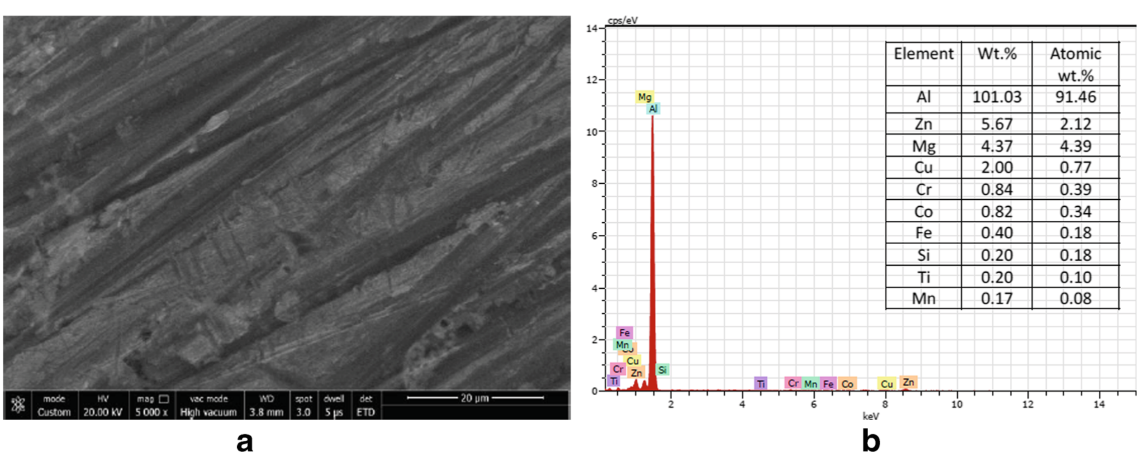

Fig. 4 Details of fabricated composite (AA7075/Co) **a** SEM micrograph of fabricated composite (AA7075/Co) **b** EDX image of fabricated composite (AA7075/Co)

Fig. 5 Multi specimen tester equipment

and 'w_r' represents weight fraction of particulate and w_m represents weight fraction of alloy material.

The Vicker micro-harness on 'C' scale (VHN) of the particulate filled alloy composite samples are evaluated as per ASTM E92 (Walter Uhltesting machine) at a load of 200 g by using Eq. 21 [30]. The hardness data at twelve points on the specimen samples are recorded, and average of such five samples are taken as final hardness value of the sample.

$$Vicker\ micro - hardness = 1.854\frac{f}{d} \quad (21)$$

where, 'f' is normal load (kg) and 'd' is the mean diagonal of the sample (mm).

3.4 Multi-Specimen Tribo-Tester

The sliding wear experimental simulation of investigated specimens are performed on multi-specimen tribo-tester (Fig. 5: Model TR-705, Ducom, Bangalore, India) as per ASTM G 99 standard. The schematic diagram of the same is shown in (Fig. 6). The tribo-tester consists of disc material of EN31 steel (60-70 HRC); speed range of 1-1400 rpm and normal load of 1-100 N respectively. The actual parameters and their values chosen for experimentation are listed in Table 2 with track diameter of 30 mm at ambient temperature. The wear losses of specimens (size: 14 × 9 × 10 mm^3) are measured both in terms of loss of vertical length (micron) automatically using LVDT transducer and weight loss by tester before/after the test run. The weight loss is measured on electronic balance having accuracy of ±0.001 mg. Thereafter, specific wear rate i.e. 'Ws' (mm^3/N-m) of the specimens are computed [31] using Eq. 22.

$$Ws = \frac{\Delta m}{\rho \cdot vs \cdot t \cdot fn} \quad (22)$$

where, Δm is mass loss (g), 'ρ' is density (gm/cc), 'v_s' is sliding velocity (m/s), 't' is the test duration (s), 'f_n' is normal load (N) respectively.

3.5 Experimental Analysis

Taguchi design of experiment is one of the optimal experimental design technique used in most of the experimental

Fig. 6 Schematic diagram multi specimen tester

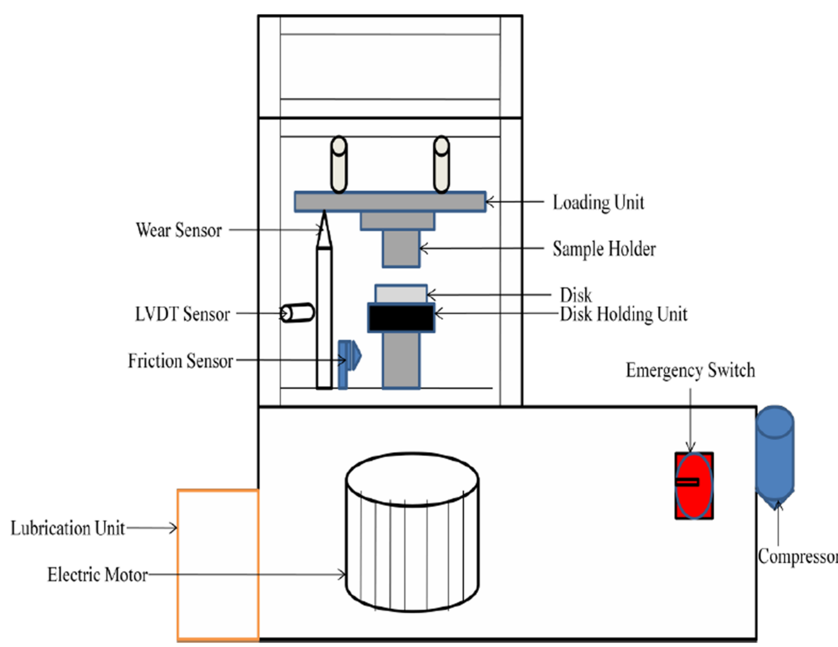

Table 2 Working range of selected parameters

Control	Level					
	I	II	III	IV	V	units
Normal Load (A)	20	35	50	65	80	N
Filler Content (B)	0	0.5	1	1.5	2	%
Sliding Velocity (C)	0.25	0.5	0.75	1	1.25	m/sec
Sliding Distance (D)	250	500	750	1000	1250	m

research work. This technique not only helps to analyze the optimal experimental results but also reported to find out the optimal factor settings. Hence, in this study L_{25} orthogonal array design has been implemented to conduct the wear analysis of the particulate filled alloy composites. The following four input parameters are taken such as: normal load (N), filler content (wt.%), sliding velocity (m/s), sliding distance (m) respectively to obtain wear rate of the unfilled and particulate filled alloy composites. In this study, smaller-is-better characteristics approach is adopted to get minimum wear of the composites by using Eq. 23 as shown below [32]. Again, after analysis of experimental work analysis of variance statistical technique is also applied to obtain the significant factor combination of the proposed alloy composites.

$$\frac{S}{N} = -10 \log \frac{1}{N} \sum Y^2 \tag{23}$$

where, N= number of experiments and Y= output performance.

3.6 Surface Morphology Studies

The micro-structural analysis of the worn samples are than analyzed by using FE-Scanning Electron Microscope (FEI Nova Nano SEM 450, USA) to understand the wear mechanism of the alloy composites for gear material application.

4 Results and Discussion

4.1 Effect of Voids Content and Hardness

Table 3 shows the result of void content of the cobalt metal particulate filled Al 7075 alloy composites obtained from theoretical and experimental densities. The void content of the alloy composites are gradually increased with the increase in filler content. This shows voids always effect the properties and ultimately the alloy shows negative effect in strength as well as wear rate also. However, as far as hardness is concerned the hardness of the particulate filled alloy composites increased with the increased in filler content (Fig. 7) and 2 wt.% cobalt filled shows maximum hardness (196HV) among the unfilled and particulate filled alloy composites. It is also observed that the hardness of particulate filled alloy composites increased in the rate of 18%, 19%, 28% and 30% higher than the base alloy. The increase in hardness is only because of presence of hard metallic particulate in the base alloy material [33] and therefore, the load transfer capacity of matrix to the reinforcement side is increased [34].

4.2 Steady State Wear Analysis

4.2.1 Effect of Sliding Velocity on Wear Rate of the Alloy Composites

Figure 8 shows the graph between specific wear rate and sliding velocity (0.25, 0.50, 0.75 and 1.00) and 1.25 m/s) for unfilled and particulate filled alloy composites under steady-state operating conditions. The remaining factors such as: sliding distance (250m) and normal load (20N) are remains constant respectively. The specific wear rate of the unfilled alloy composite increases with the increase in sliding velocity from 0.25m/s to 1m/s, whereas the particulate filled alloy composites the specific wear rate remaining constant with the increased in sliding velocity up to 1m/s after that slightly increased the wear rate up to 1.25m/s respectively. Therefore, the effect of the particulate

Table 3 Comparison of Experimental Density and Theoretical Density

Sl. No.	Composition	Theoretical density (gm/cc3)	Experimental density (gm/cc3)	Void Content (%)
1	0 wt.-% Co	2.90	2.86	1.379
2	0.5 wt.-% Co	2.91	2.80	3.780
3	1.0 wt.-% Co	2.92	2.77	3.136
4	1.5 wt.-% Co	2.93	2.69	8.191
5	2.0 wt.-% Co	2.94	2.65	9.863

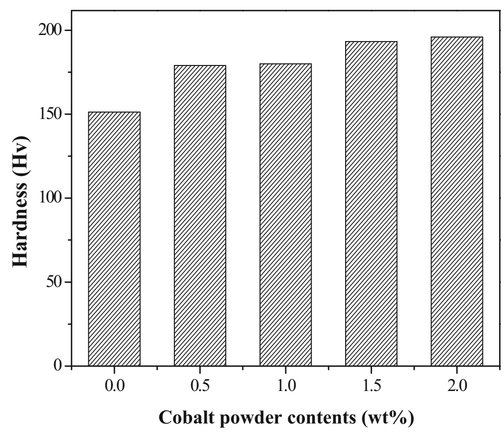

Fig. 7 Effect of hardness on Cobalt metal powder filled al 7075 al alloy composite

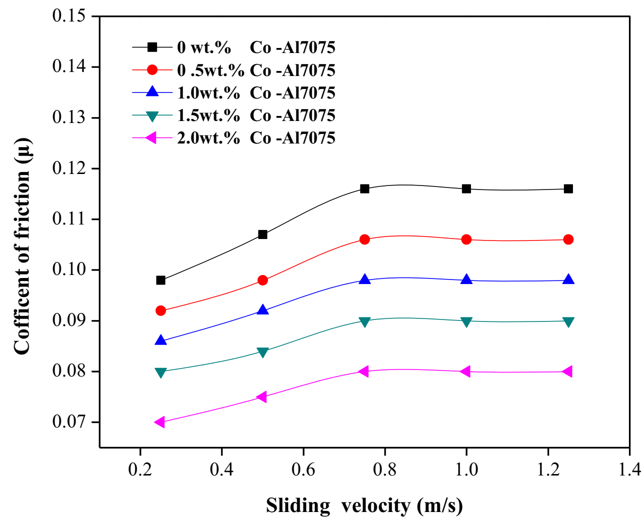

Fig. 9 Effect of sliding velocity on coefficient of friction of Co filled Al7075 alloy Composites

filled alloy composites with the increase in hardness the wear rate remaining constant irrespective of change in sliding velocity up to 1m/s but on higher sliding velocity all the particulate filled alloy composites the wear rate shows in an increasing order [35]. Jin et al. [36] observed similar trends while studying dry sliding wear behavior for $Mg_2B_2O_5$ whisker reinforced Al 6061matrix composites may be due to better wetability between ingredients.

Similarly, as far as coefficient of friction is concern the value of the coefficient of friction (COF) increases with the increased in weight percentage of the composite (Fig. 9). 1.5 wt.% of Co filled Al7075 alloy composite shows highest value of COF which is 0.116 at 0.75 m/s sliding velocity; for other weight fractions also shown approximately constant value of COF from 0.75 m/s to 1.25 m/s sliding velocity. Initially, COF value increases from 0.25 m/s to 0.5 m/s but on higher velocity the value of COF remains constant. The increased in COF may be due to hard asperities act such as cutting tool which can be rub the surface of material in particular kind of scratch or grooves in the presence of hard reinforcing particulate from worm surface of composite material. There is another reason that plastic deformation between the sample material and disk surface can be responsible for the greater value of COF [38, 39].

4.2.2 Effect of Normal Load on Wear Rate of the Alloy Composites

Figure 10 shows the specific wear rate vs normal load of particulate filled alloy composites under steady state operating condition. The results observed that with the increase in normal load the wear rate of the unfilled and particulate filled alloy composites gradually decreases

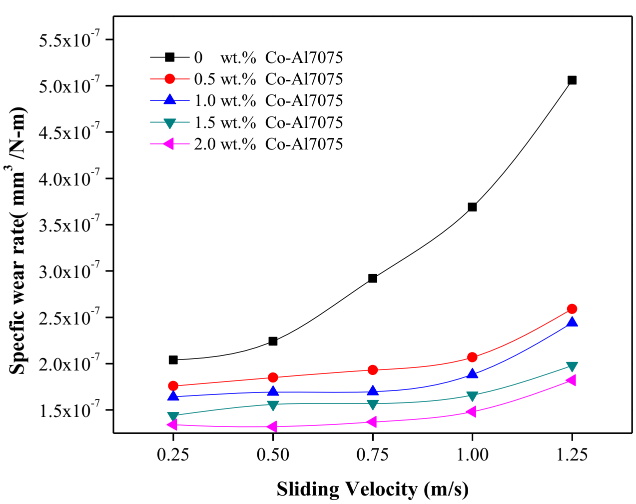

Fig. 8 Effect of sliding velocity on specific wear rate of Co filled Al7075 alloy composites

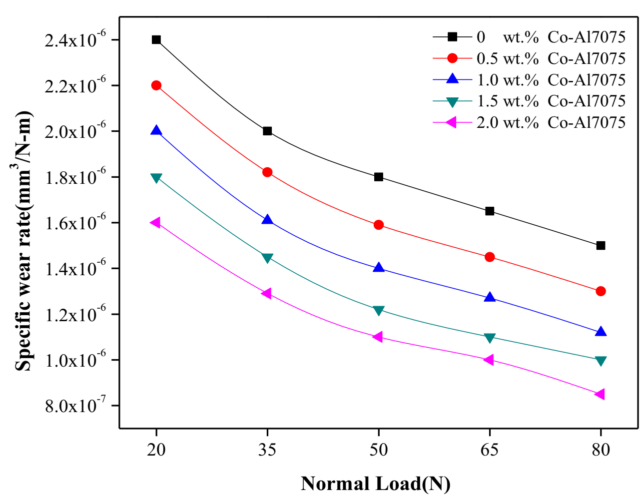

Fig. 10 Effect normal load on specific wear rate of Co filled Al7075 alloy composites

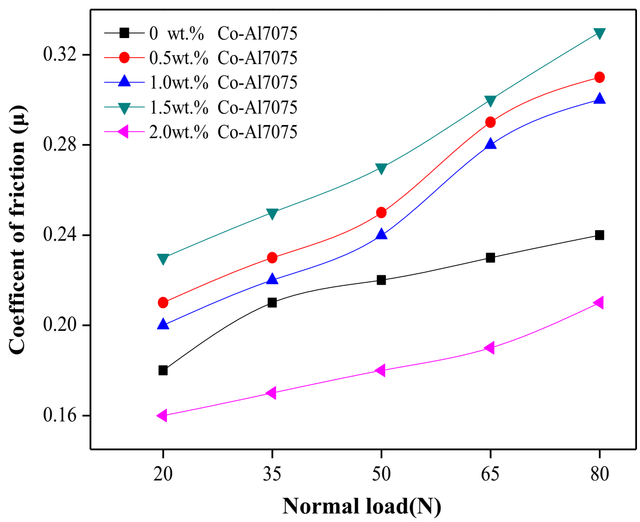

Fig. 11 Effect normal load on coefficient of friction of Co filled Al7075alloy composites

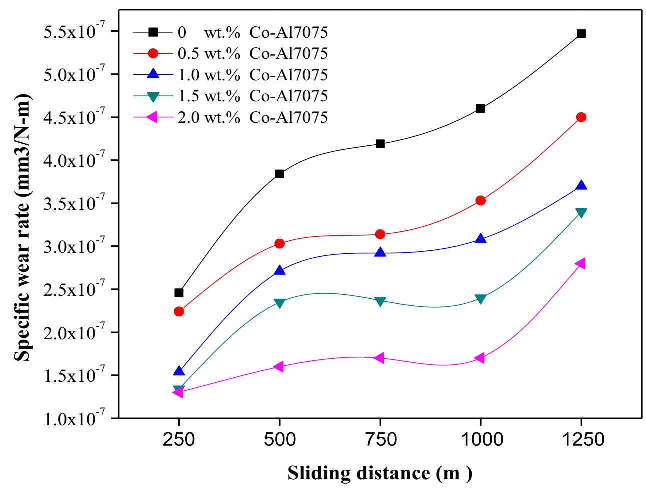

Fig. 12 Effect sliding distance on specific wear rate of Co filled Al7075 alloy composites

irrespective of variation of filler content. This is due to development of lubricant at the interface of pin material and the counter disc materials at higher load. Similar, study was also reported by Kongjie Jin, et al. [40]. Baskaranet al. [41] of TiC particulate filled Al 7075 alloy composites at different loading conditions and proposed that these materials wear resistance capacity was quite high at higher load. Again, from this analysis the coefficient of friction graph is also observed with respect to normal load for all the unfilled and particulate filled alloy composites and shows an increased in trend with the increase in normal load (Fig. 11). It is also noticed that the value of CoF improves at lower load but at higher normal load, cracking of this mechanically mixed layer take place and the resultant hard debris via plowing action on the counter surface result in higher COF [42, 43].

4.2.3 Effect of Sliding Distance on Wear Rate of the Alloy Composites

The wear rate of the specimen samples are plotted against the sliding distance for particulate filled Al7075 aluminium alloy composites (Fig. 12). In general, the specific wear rate is observed in an increasing trend with the increasing in sliding distance across the composition [44]. It may be due to the fact contact the region of sliding surface raised with increased in contact time which in convert increased wear of the composite [6]. Figure 13 represents the effect of sliding distance on COF for cobalt particulate filled aluminium alloy composite. It is evident from Fig. 13 that the coefficient of friction increases with the increased sliding distance of cobalt particulate filled aluminium alloy composite. It noticed that the coefficient of friction value is maximum at 0 wt.% Co and minimum value at 2 wt.% Co content. Specific wear rate of composite is slowly increased with increasing in sliding speed. Consequently, the results indicate that the obtained wear resistance with hardness in heat treatment has disappeared through grain growing mechanism [44].

4.3 Taguchi Design Experimental Analyses

Finally, Taguchi design of experiment technique is implemented in the present proposed unfilled and particulate filled alloy composites and the level of parameters are selected based on the steady-state-experimental analysis. In this study, L_{25} orthogonal array design of experimental

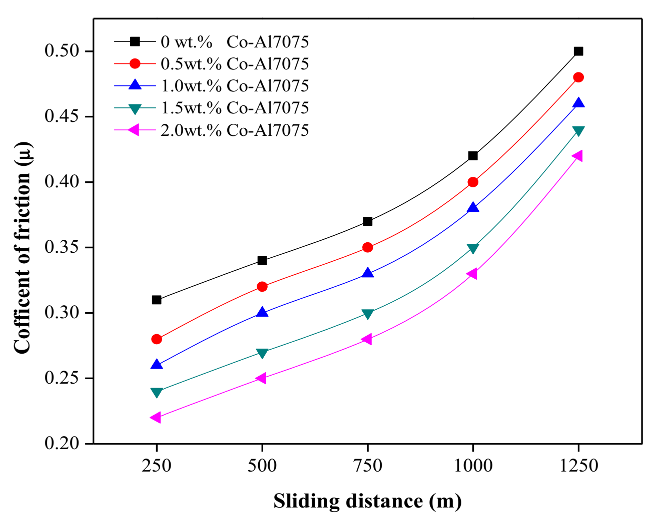

Fig. 13 Effect of sliding distance on coefficient of friction of Co Filled Al7075Alloy Composites

Table 4 Experimental layout of L25 orthogonal array

Expt. No	Normal load (N)	Filler Content (Wt %)	Sliding Velocity (m/sec)	Sliding Distance (m)	Specific wear rate (mm3/N-m)	S/N Ratio (db)
1	20	0	0.25	250	2.606E-06	111.681
2	20	0.5	0.50	500	2.471E-07	132.143
3	20	1.0	0.75	750	1.048E-07	139.593
4	20	1.5	1.0	1000	1.910E-07	134.379
5	20	2.0	1.25	1250	6.426E-07	123.841
6	35	0	1.0	250	2.632E-07	131.594
7	35	0.5	1.25	750	1.583E-07	136.010
8	35	1.0	0.25	1000	1.284E-07	137.829
9	35	1.5	0.50	1250	2.208E-07	133.120
10	35	2.0	0.75	250	1.284E-07	137.829
11	50	0	0.50	750	1.138E-07	138.877
12	50	0.5	0.75	1000	6.563E-06	103.658
13	50	1.0	1.0	1250	1.492E-07	136.525
14	50	1.5	1.25	250	6.292E-08	144.024
15	50	2.0	0.25	500	1.437E-07	136.851
16	65	0	1.25	1000	9.334E-08	140.599
17	65	0.5	0.25	1250	1.244E-07	138.104
18	65	1.0	0.5	250	5.531E-08	145.144
19	65	1.5	0.75	500	2.627E-07	131.611
20	65	2.0	1.00	750	2.535E-08	151.920
21	80	0	0.75	1250	2.067E-07	133.693
22	80	0.5	1.0	250	1.460E-07	136.713
23	80	1.0	1.25	500	1.966E-08	154.128
24	80	1.5	0.25	750	4.307E-08	147.317
25	80	2.0	0.5	1000	3.370E-08	149.447

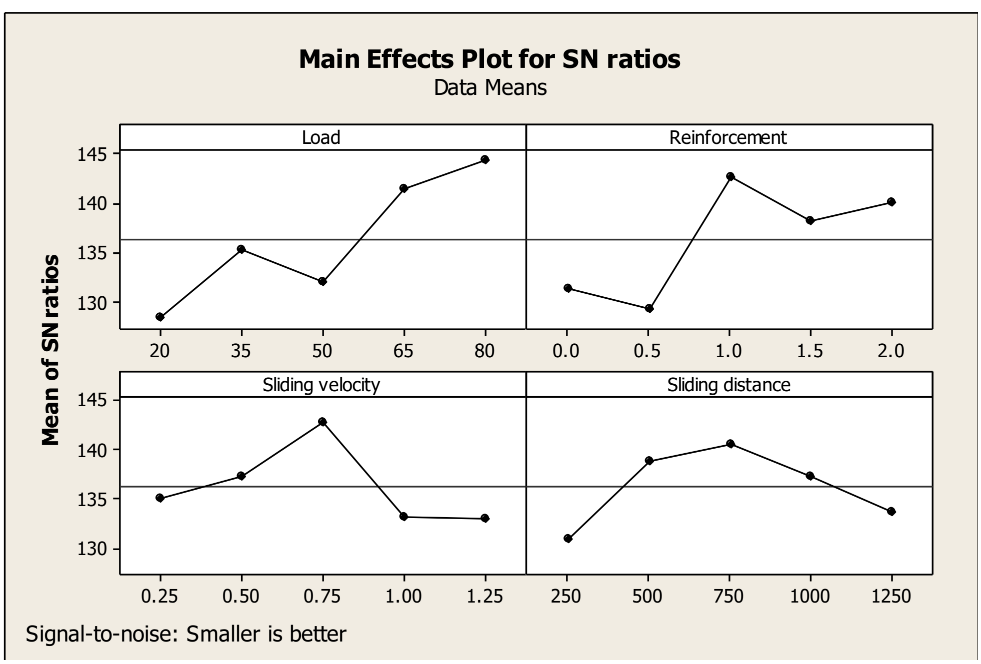

Fig. 14 Effect of Control factors on wear rate For Co filled Al7075 alloy Composites

Table 5 Calculation of theoretical specific wear rate of Co filled 7075 Aluminium alloy Composites

Expt. No	Normal load (N)	Filler Content (wt. %)	Sliding Velocity (m/sec)	Sliding Distance (m)	Experimental specific wear rate (mm3/N-m)	Theoretical specific wear rate (mm3/N-m)	% Error
1	20	0	0.25	250	2.606E-06	2.690E-06	3.12
2	20	0.5	0.50	500	2.471E-07	2.585E-07	4.41
3	20	1.0	0.75	750	1.048E-07	1.100E-07	4.72
4	20	1.5	1.0	1000	1.910E-07	2.000E-07	4.50
5	20	2.0	1.25	1250	6.426E-07	6.546E-07	1.83
6	35	0	1.0	250	2.632E-07	2.752E-07	4.36
7	35	0.5	1.25	750	1.583E-07	1.623E-07	2.46
8	35	1.0	0.25	1000	1.284E-07	1.311E-07	2.05
9	35	1.5	0.50	1250	2.208E-07	2.288E-07	3.49
10	35	2.0	0.75	250	1.284E-07	1.324E-07	3.02
11	50	0	0.50	750	1.138E-07	1.188E-07	4.20
12	50	0.5	0.75	1000	6.563E-06	6.652E-07	1.33
13	50	1.0	1.0	1250	1.492E-07	1.524E-07	2.09
14	50	1.5	1.25	250	6.292E-08	6.392E-07	1.56
15	50	2.0	0.25	500	1.437E-07	1.492E-07	3.68
16	65	0	1.25	1000	9.334E-08	9.432E-07	1.03
17	65	0.5	0.25	1250	1.244E-07	1.284E-07	3.11
18	65	1.0	0.5	250	5.531E-08	5.652E-08	2.14
19	65	1.5	0.75	500	2.627E-07	2.697E-07	2.59
20	65	2.0	1.00	750	2.535E-08	2.653E-08	4.44
21	80	0	0.75	1250	2.067E-07	2.107E-07	1.89
22	80	0.5	1.0	250	1.460E-07	1.520E-07	3.94
23	80	1.0	1.25	500	1.966E-08	2.033E-08	3.29
24	80	1.5	0.25	750	4.307E-08	4.423E-08	2.62
25	80	2.0	0.5	1000	3.370E-08	3.540E-08	4.80

Table 6 ANOVA table for specific wear rate (Co filled Al7075 alloy Composite)

Source	DF	Seq SS	Adj SS	Adj MS	F	P
Load	4	866.8	866.8	216.7	2.17	0.164
Reinforcement	4	653.6	653.6	163.4	1.63	0.257
Sliding velocity	4	320.9	320.9	80.2	0.80	0.577
Sliding distance	4	305.5	305.5	76.4	0.76	0.588
Error	8	800.5	800.5	100.1		
Total	24	2947.3				

technique (MINITAB 16 software) is implanted by taking four parameters at-a-time with five levels each factor. The wear rate of the alloy composites is converted it into signal-to-noise ratio (S/N ratio), by adopting smaller-is-better characteristics in order to minimize the wear rate of the alloy composites. The detail of the experimental results along with their respective S/N ratio values is presented in Table 4 and the corresponding level of significance of each factor is presented in Fig. 14.

4.4 Comparison of Theoretical Results with Experimental Results for Wear Rate of the Alloy Composites

Finally, the confirmation test is performed to cross verify the predicted results with the experimental one by the proposed specific combination of level of each factor to obtain the wear rate of the alloy composites. The detail factor combinations along with the predictive as well as

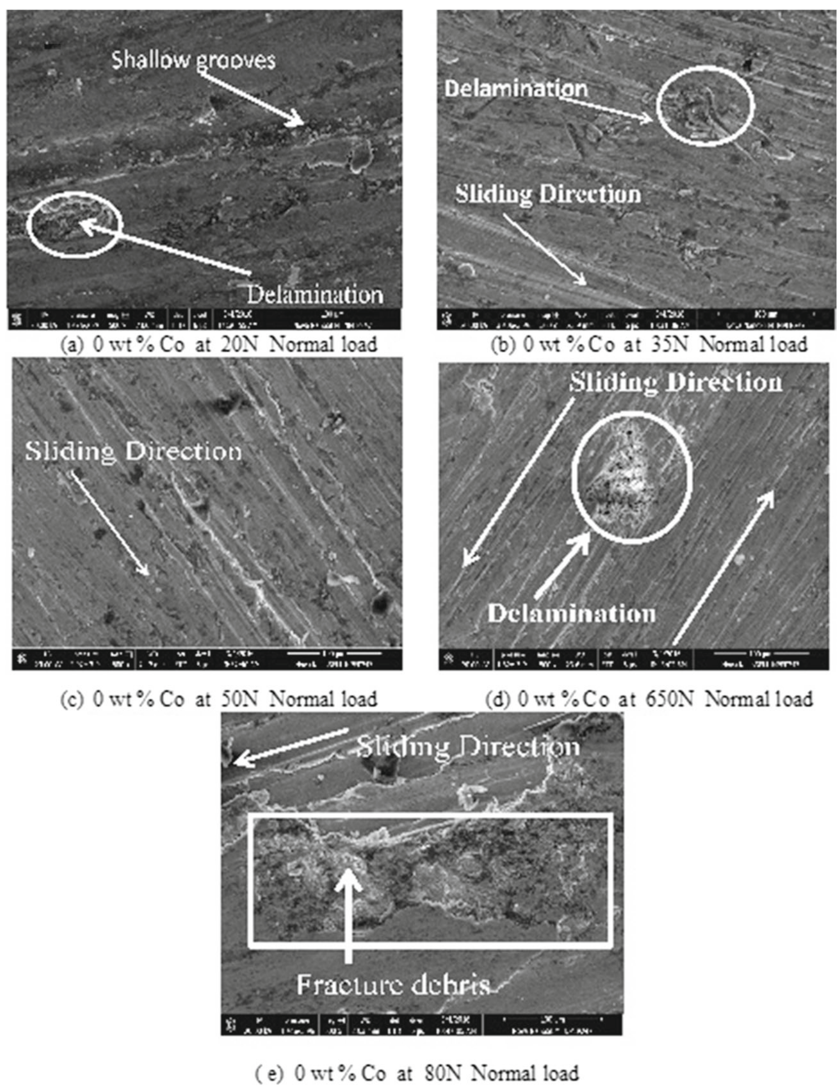

Fig. 15 Surface micrographs of Co filled Al 7075 alloy composite with varying normal load (keeping other factors constant such as sliding speed0.25 m/s, sliding distance 250 m)

experimental results are reported in Table 5. It found that minimum error shows at higher load and higher sliding velocity whereas, maximum error shows at lower load and velocity respectively. The maximum error lies between the range of 1 to 5% from the proposed theoretical model with the experiment wear rate results. Hence, the proposed model could potentially be used as an efficient tool to predict the specific wear rate of the composites for gearing applications.

4.5 ANOVA Analysis

The outcome of analysis of variance (ANOVA) is shown in Table 6 and the level of significance is taken 5% for 95% confidence level. The parameter ‘P’ represents percentage contribution for an individual factor as is shown in Table 6. It is observed that the normal load has P = 0.164 contribution, sliding distance having P = 0.588 contribution, sliding velocity having p= 0.577 contribution and reinforcement having P = 0.257 contribution respectively. The conclusive order of contribution to determine the specific wear rate is: Sliding distance>Sliding velocity>Reinforcement>Load.

4.6 Worn Out Surface Morphology

The prevailing wear mechanisms resulting surface tribology of worn surface of the specimen composite samples are shown in Figs. 15, 16, 17, 18. The wear morphology Fig. 15 (normal load of 20 - 80N, sliding velocity of 0.25 m/s, sliding distance of 250 m) shows highest specific wear rate at steady state condition. The plot Fig. 9 shows highest specific wear rate for lower normal load i.e. 20 N. Figure 15a shows the worn surface morphology of the base alloy material operated under constant normal load (20 N), sliding velocity (25 m/s) and sliding distance (250 m) respectively (See Fig. 9). It shows number of shallow

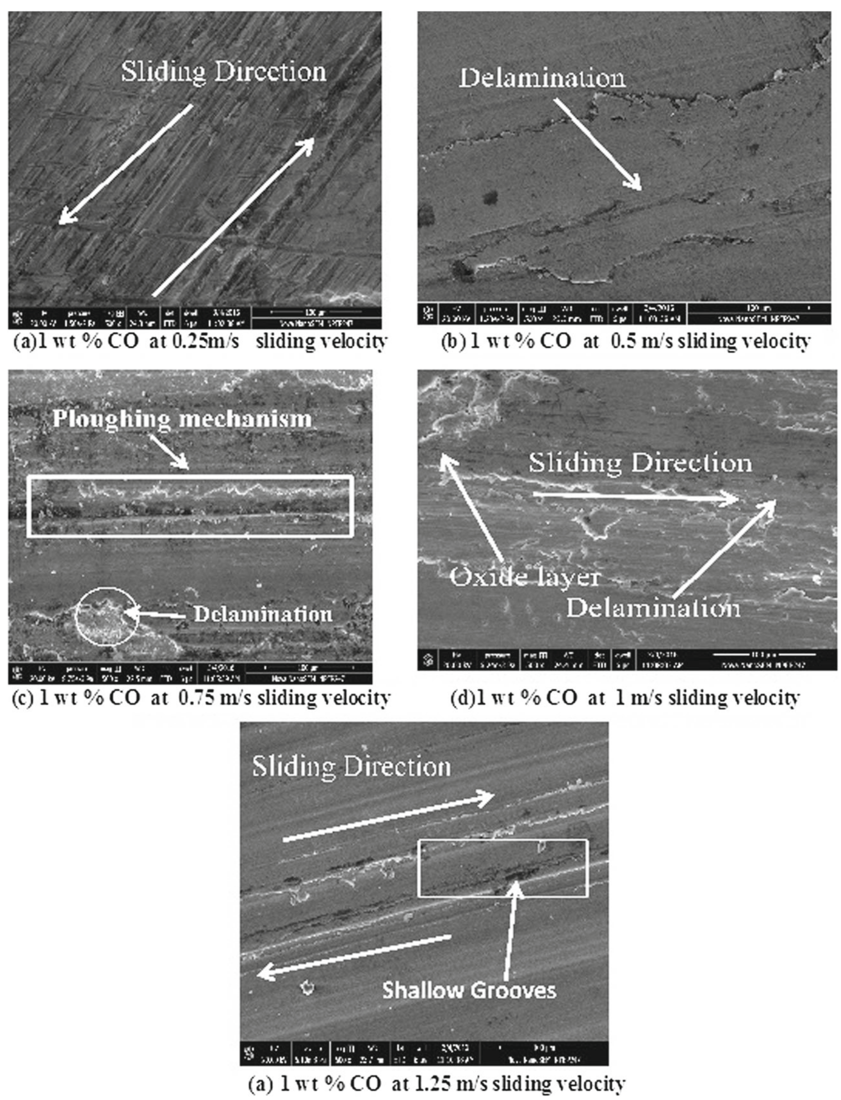

Fig. 16 Surface micrographs of Co filled Al 7075 alloy composite with varying sliding speed (keeping other factors constant such as normal load 20 N, sliding distance 250 m)

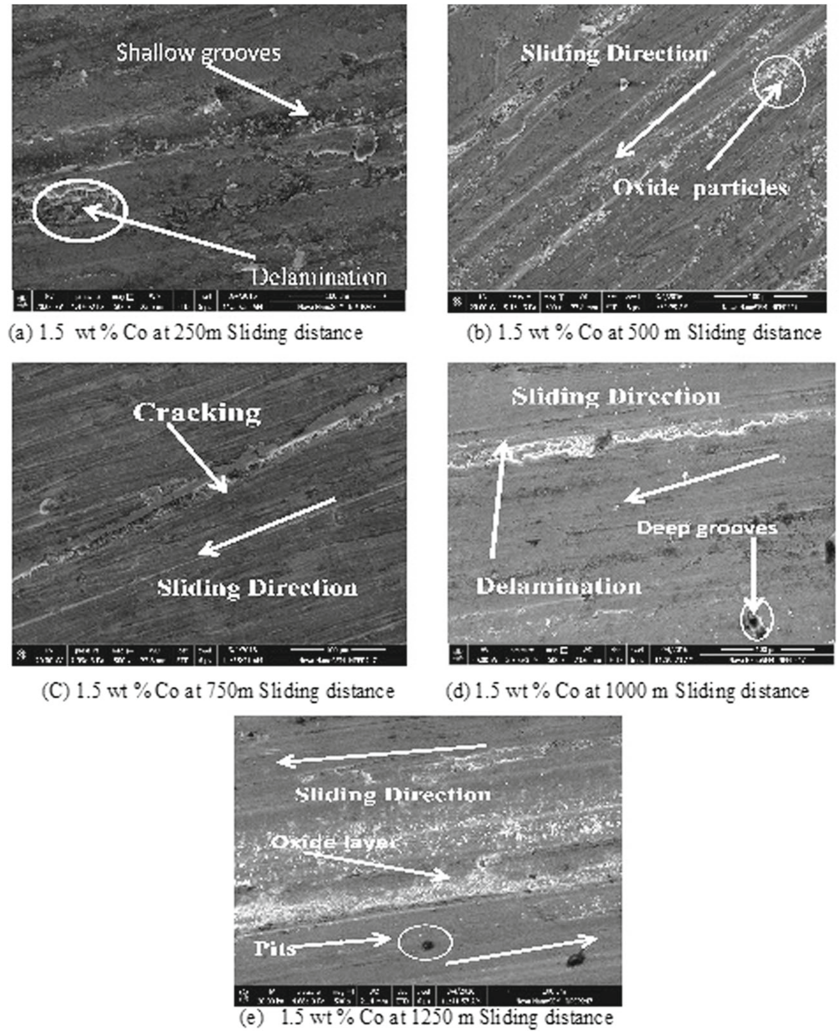

Fig. 17 Surface micrographs of Co filled al7075 alloy composite materials varying sliding distance (keeping other factors constant such as normal load 20 N, sliding velocity 0.25 m/s)

grooves because of the presence of higher void content 9.863%, resulting in week interfacial bonding between the particulates and matrix; consequently lead to removal of material from surface in-form-of groves. Figure 15c shows the regular and continuous wear marks [48] along the sliding direction. Increase in normal load with specific were rate of unfilled alloy decrease compared to higher wt.% of all prepared specimen composites. In the sliding wear method, when the load are applied on the sample then when the contact between pin and counter face shows the friction heat is increased which is influenced by normal load, from the Fig. 15d shows the presence of delamination and sliding direction due to the formation of debris. However at the 65 N load and sliding speed 0.25 m/s lager region compacted layer demolition enters which would create abrasive wear, resulting in the greatest coefficient of friction [42].

In the above study, it may be concluded that at the staring of type III wear system, adhesive and abrasive wear process are very needful mechanism which will towards the creation of compacted layer under higher load and then it play the important role of three-body abrasive wear and oxidative wear mechanisms. The worn surface also represents fractured particles of fillers and the matrix, which promotes high loss of materials and delamination occurs higher normal load and higher velocity (Fig. 15e) [45].

Figure 16 shows the surface micrographs via steady state condition with changing sliding speed while putting other parameters fixed like normal load 20 N, sliding distance 250 m. The Figure 16a–b shows wear surface of metal matrix composite at 1 wt.% Co at 0.25 m/s sliding velocity and other parameters like normal load, sliding distance at constant. In sliding process, good eutectic Cobalt phase forms a poor interface with matrix and the filler with alloy composite and unfilled alloy is developed a better bond due to improved the wear resistance. Depend on the friction coefficient analysis and according to the worn out surface of the 1 wt.% Co samples, the wear mechanism is a single abrasion wear under the applied both load [33]. Similarly,

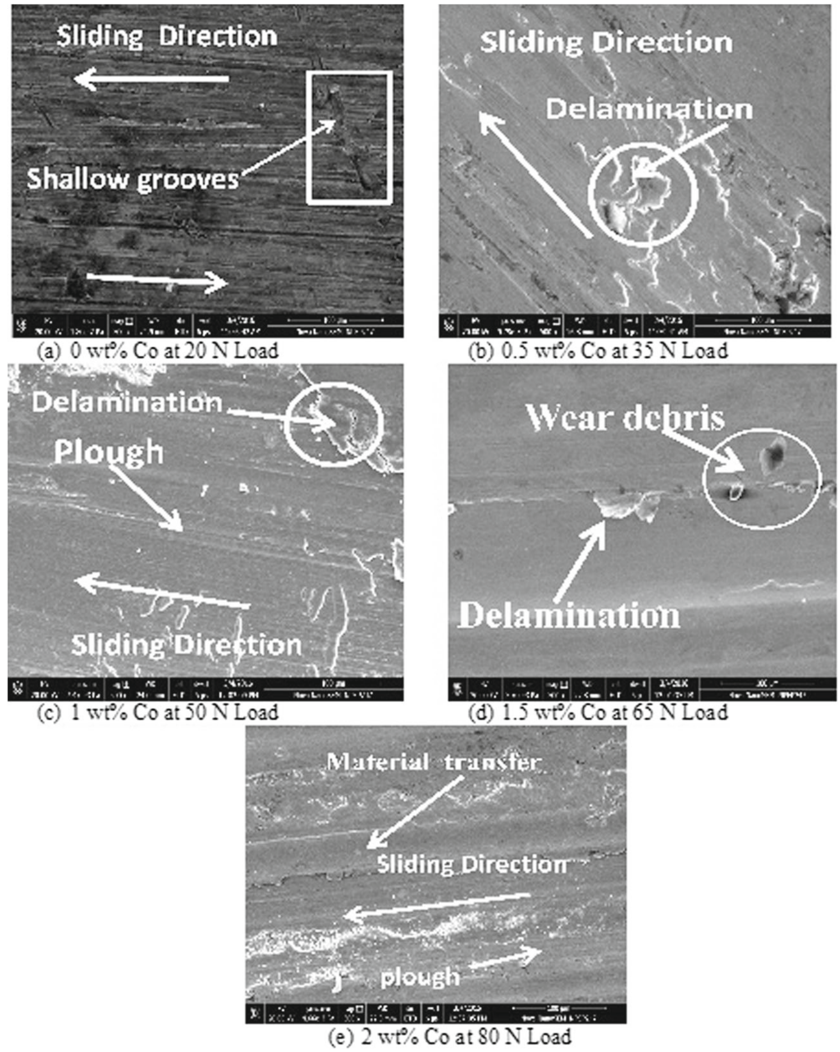

Fig. 18 Micrographs of the highest SWR of the composite materials under L25 Taguchi design of experimental test runs

the delamination wear occurs at the more normal load and more velocity and there may be another reason that the delamination wear occurs at formation of wear debris shown in Fig. 16b [45]. Figure 16c shows the presence of plough mechanism due to the highest wear rate and delamination wear generate at highest load and highest velocity. The highest sliding velocity depicts the maximum wear rate for 0 wt.% of Co filled aluminum alloy composite materials [41]. In Fig. 16d–e show specific wear rate under lower sliding velocity and load, it appears that fine debris forms easily. The debris of oxygen-rich will be due to slight raise of friction coefficient and wear rate [37]. Hence, in type first wear system; oxidative wear is the controlling wear process. Delamination wear occurs at more applied load and more applied velocity the highest velocity gives the more wear rate for 0 wt.% of Co filled aluminum alloy composite materials [34]. Such oxide debris on the surface may be generated via the adhesion and micro-cutting. Therefore, the changing of a wear rate and coefficient of friction is strongest via micro-cutting, adhesion and severe plastic deformation [46].

Figure 17, represents the surface micrographs via steady state condition with changing sliding distance while putting other factors fixed such as normal load 20 N, sliding velocity 0.25 m/s.

Figure 17a–b represents the SEM image of the worn out surfaces of 1.5 wt.% Co metal powder reinforced aluminum composite after sliding 250 m and 500 m distance at 0.25 m/s and 20 N normal load. Figure 17a depicts flat surface with grooves and few content of delamination generates owing to lesser frictional heating between the mating surfaces and in Fig. 17b shows large amount of oxide particle in debris over the specimen surface, may be due to delamination of oxide layers at lower normal load and lower sliding velocity.

In Fig. 17c–d shows the presences of deep grooves, big content delamination and crack due to higher friction heat that accelerate wear rate and increases surface roughness

[47]. Figure 17e shows wear scars stick fast to the sliding surface owing to compaction of particles situated directly below the counter face and it is noticed that more plastic flow grows the shear stress need to peel off wearing surface and motivates delamination wear mechanism. The oxide layer and adhesive compact particles on worn surfaces clearly restricts intense plastic deformation there by less wear loss.

The studies of Co metal powder filled Al7075 alloy composite materials L_{25} Taguchi design experimental trial runs are employed in Fig. 18. Figure 18a shows relatively flat surface with grooves along with large ploughing of counter surface of pin sample and mild wear mechanism occurs at lower applied normal load and lower sliding velocity of the composite alloy. The shallow grooves occur due to few applied load and less sliding velocity [45]. The micrograph (Fig. 18b) for 0.5 wt.% of Cobalt metal powder reinforced alloy composites materials represents the highest SWR (Experiment run 7, Table 5) at 1.25 m/s of sliding velocity, 35 N of loads and 750 m of sliding distance at a room environment.

When two surfaces of disk and pin specimen were rubbed together throughout sliding wear method at 1.25 m/s sliding velocity, heat is developed at counter face and therefore particulate strong cobalt particles released from the base material. Higher wear rate obtained by Delamination phenomenon. Delamination wear are generated by the higher load and higher velocity and when the two surfaces are rubbed together during the sliding velocity, more amount of heat friction is gent rated at counter face [45].

Figure 18c represents the micrograph for 1 wt.% Co metal powder filled 7075 aluminum matrix which represents more wear rate (Experiment run 13, Table 5) with sliding velocity at 1 m/s. Normal load 50 N over the sliding distance of 1250 m. The micrograph represents delamination, plough were created throughout the sliding method. Delamination and plough of worm surface were noticed under the higher load condition. A almost same occurrence of delamination is also investigated at 1.5 wt.% of Co filled Al7075 alloy composite material where the higher specific wear rate (experiment trial run 19, Table 5) are noticed with 0.75 m/s of sliding velocity, 65 N of load and 500 m of sliding distance are depicted in Fig. 18d. The micrograph as represents in Fig. 18e for 2 wt.% Co metal powder reinforced Al7075 aluminium matrix against (Experiment run 25, Table 5) for a sliding velocity of 0.5m/s and load 80N at minimum wear rate. Filler particulates i.e. wear debris pulled off the pin surface during sliding velocity at high sliding velocity [49].

The micrograph shown in Fig. 18e for 2 wt.% Co metal powder filled Al7075 alloy (Experiment run 25, Table 5) studied under a sliding velocity of 5m/s, load 80N shows minimum wear rate. As sliding velocity increase, filler particulates pulled off in form of wear from the pin surface [49] causing sever wear as shown in Fig. 16e. This may results in heavy plastic formation that adheres to worn surfaces and responsible for higher COF. Simultaneously, such debris gets compacted against the rubbing surface leading to the formation of tribo-layer [46].

4.7 Conclusions

The study of mechanical and wear behavior of Cobalt metal powder filled Al 7075 alloy composites gives below conclusions:

- The Co metal powder reinforcement in aluminium alloy Composites fabricated using high temperature vacuum casting exhibits improved wear resistance thus may be used as potential gear material.
- The void content found to be increasing from 1.379 to 9.863% up to 10 wt.% of Co filler particles. However, the hardness of the filled alloy composites increases up to 2 wt.% of Co metal powder filler particles i.e. 196HV.
- The specific wear rate said alloy composites increases with sliding velocity under steady state conditions. The order followed is: 0 wt.% Co>0.5 wt.% Co>1 wt.% Co>1.5 wt.% Co>2 wt.% Co while, COF follows 1.5 wt.% Co>2 wt.% Co>1 wt.% Co>0.5 wt.% Co>0 wt.% Co order respectively.
- The specific wear rate of said alloy composites decreases with normal load (20-80 N) under steady state conditions. The order followed as : 0.5 wt.% Co>1 wt.% Co>2 wt.% Co>1.5 wt.% Co>0 wt.% Co irrespective of the normal load condition.
- ANOVA results shows that input factors that controls wear performance of alloyed composites are in order of sliding distance (D) [$p = 0.588\%$] >Sliding velocity(C) [$p = 0.577\%$] >Reinforcement (B) [$p = 0.257\%$] >Normal load (A) [$p = 0.164\%$]. It means that sliding distance is the most prominent variable controlling the specific wear rate of alloyed composites.
- FESEM micrographs reveal the wear mechanism responsible for wear rate behaviors of investigated alloy composites under set of different experimental input variables.

Acknowledgments The authors acknowledge financial support drawn from Malaviya National Institute of Technology Jaipur, Jaipur-302017, Rajasthan INDIA. The authors also acknowledge the facilities provided by Material Research Center and Advanced Research Centre for Tribology for characterization and experimentation.

Compliance with Ethical Standards

Conflict of interests The author(s) declared no potential conflicts of interests with respect to the research, authorship, and publication of this article

References

1. Ramnath B, Elanchezhian C, Jaivignesh M (2014) Mater Des 58:332–338
2. Ralph B, Yuen HC, Lee HC (1997) J Mater Process Technol 63:339–353
3. Kumar GB, Rao CSP, Selvaraj N (2011) J Miner Mater Char Eng 10:59–91
4. Gangwar S, Kukshal V, Patnaik A (2012) Int J Compos Mater 3:69–72
5. Kukshal V, Gangwar S, Patnaik A (2013) J Mater Design Appl. https://doi.org/10.1177/1464420713499514
6. Baradeswaran A, Perumal E (2013) Compos Part B 54:146–152
7. Kumar GB, Rao CSP, Selvarajet N (2010) J Miner Mater Char Eng 99(1):43–55
8. Komai K, Minoshima K, Ryoson H (1993) Compos Sci Technol 46(1):59–66
9. Savaskan T, Alemda Y (2010) Wear 268:56
10. Rajeev VR, Dwivedi DK, Jain S (2009) Tribol Online 4(5):115–126
11. Baradeswaran A, Perumal A, Issac FR (2013) Procedia Eng 64:973–982
12. Ravindran P, Manisekar K, Narayanasamyet R (2013) Ceram Int 39:1169–1182
13. Kumar R, Dhiman S (2013) Mater Des 50:351–359
14. Li X, Sosa M, Olofsson U (2015) Wear 340(341):31–40
15. Kran TS, Kumar MP, Basavarajappa S, Viswanatha BM (2014) Mater Des 63:294–304
16. Nwambu CN, Nnuka EE, Odo JU, Nwoye CI, Nwakpa SO (2014) Int J Eng Sci Invent 3:20–24
17. Sani AS, Aliyu I, Polyerp E (2012) Int J Sci Eng 3(12):2229–2318
18. Haq UIMI, Anand A (2018) Silicon. https://doi.org/10.1007/s12633-017-9675-1
19. Kumar A, Patnaik A, Bhat IK (2017) Powder Metallurgy. https://doi.org/10.1080/00325899.2017.1318481
20. Kumar A, Patnaik A, Bhat IK (2018) Appl Mech Mater 877:118–136. ISSN: 1662–7482
21. Lim SC, Ashby MF (1987) Acta Metal 35(1):1–24
22. Suh NP (1973) Wear 25:111–124
23. Quinn TFJ (1962) Br J Appl Phys 13:33–33
24. Archard JF (1953) J Appl Phys 24:981–988
25. Kogut L, Etsion I (2002) J Appl Mech-T ASME 69(5):657–662
26. Chang WR, Etsion I, Bogy DB (1987) J Tribol-T ASME 109:257–263
27. Zhao Y, Maletta DM, Chang L (2000) J Tribol-T ASME 122:86–93
28. Wu S, Cheng HS (1993) J Tribol 115:493–500
29. Agarwal BD, Broutman LJ (1990) 2nd edn. Wiley, New York
30. Kumar SS, Devaiah M, SeshuBai V (2012) Ceram Int 38:1139–1147
31. Metals-Mechanical Testing (2000) West Conshohocken, PA
32. Siddhartha V, Patnaik A, Bhatt AD (2011) Mater Des 32(2):615–627
33. Kumar RS, Murugan N, Dinaharan I (2013) Mater Char 84:16–27
34. Reddy MS, Soma R (2014) Procedia Mater Sci 5:508–516
35. Vencla A, Rajkovic V, Zivic F (2000) Appl Surf Sci 280:646–654
36. Jin P-P, Chen G, Li H (2014) Trans Nonferrous Met Soc China 24:49–57
37. Zhang L, He XB, Qu XB (2008) Wear 265(11–12):1848–1856
38. Renza A, Khadera I, Kailera A (2016) J Eur Ceram Soc 36:705–717
39. Kongjie J, Zhuhu Q, Shengyu Z (2016) Tribol Int 96:132–140
40. Baskaran S, Anandakrishnan V, Muthukannan D (2014) Mater Des 60:184–192
41. Qing-ju (2006) Trans Nonferrous Met Soc China 16:1135–1140
42. Kumar N, Gautam G, Gautam RK (2016) Tribol Int 97:313–326
43. Feyzullah LU, Ertürk AT, Güven EA (2013) Trans Nonferrous Met Soc China 23:3575–3583
44. Cui X, Wu Y, Liu X (2015) J Mater Sci Technol 31:1027–1033
45. Chi H, Jiang L, Chen G (2015) Mater Des 87:960–968
46. Ozden S, Ekici R, Nair F (2007) Compos Part A 38:484–494
47. Antony C, Kumar V, Rajadurai JS (2016) Trans Nonferrous Met Soc China 26:63–73
48. Lin N, Xie F, Yang H (2012) Appl Surf Sci 258:4960–4970
49. Kim SW, Lee UJ, Han SW, Kim DK, Ogi K (2003) Compos Part B 34:737–745